ELSEVIER

Journal of Computational and Applied Mathematics 125 (2000) 83–92

JOURNAL OF COMPUTATIONAL AND APPLIED MATHEMATICS

Performance of two methods for solving separable Hamiltonian systems

V. Antohe *, I. Gladwell

Department of Mathematics, Southern Methodist University, Dallas, TX 75275, USA

Received 15 December 1999; received in revised form 19 March 2000

Abstract

We make qualitative comparisons of fixed step symplectic and variable step nonsymplectic integrations of the separable Hénon–Heiles Hamiltonian system. Emphasis is given to interesting numerical phenomena. Particularly, we observe the relationship of the error in the computed Hamiltonian to the presence and absence of chaos, when computing with a symplectic (fixed step) method, qualitative phenomena in the Hamiltonian error for a variable step method, and the sensitivity of the chaotic behavior and of the computation of features in Poincaré sections to very small changes in initial conditions, step sizes and error tolerances. © 2000 Elsevier Science B.V. All rights reserved.

1. Introduction

Assume the autonomous Hamiltonian $H(\boldsymbol{p},\boldsymbol{q})$ is a smooth real function where $\boldsymbol{p}$ represents the generalized momenta and $\boldsymbol{q}$ the generalized coordinates, and $(\boldsymbol{p}^{\mathrm{T}},\boldsymbol{q}^{\mathrm{T}})=(p_1,p_2,\ldots,p_d,q_1,q_2,\ldots,q_d)$; d is the number of degrees of freedom. The Hamiltonian system corresponding to $H(\boldsymbol{p},\boldsymbol{q})$ is

$$\frac{\mathrm{d}p_i}{\mathrm{d}t}=-\frac{\partial H}{\partial q_i},\quad \frac{\mathrm{d}q_i}{\mathrm{d}t}=\frac{\partial H}{\partial p_i},\quad i=1,2,\ldots,d \tag{1}$$

and we need initial conditions $\boldsymbol{p}(t_0)=\boldsymbol{p}_0$, $\boldsymbol{q}(t_0)=\boldsymbol{q}_0$. Note that $H(\boldsymbol{p},\boldsymbol{q})$ is constant with time (i.e., $\mathrm{d}H/\mathrm{d}t=0$).

A separable Hamiltonian has the structure

$$H(\boldsymbol{p},\boldsymbol{q})=T(\boldsymbol{p})+V(\boldsymbol{q}). \tag{2}$$

In mechanics, $T=\frac{1}{2}\boldsymbol{p}^{\mathrm{T}}M^{-1}\boldsymbol{p}$ represents kinetic energy (M is the mass matrix) and V potential energy. The Hamiltonian system has 'partitioned form':

$$\frac{\mathrm{d}\boldsymbol{p}}{\mathrm{d}t}=-\nabla_{\boldsymbol{q}}V,\qquad \frac{\mathrm{d}\boldsymbol{q}}{\mathrm{d}t}=\nabla_{\boldsymbol{p}}T=M^{-1}\boldsymbol{p}. \tag{3}$$

* Corresponding author.

PII: S0377-0427(00)00460-X

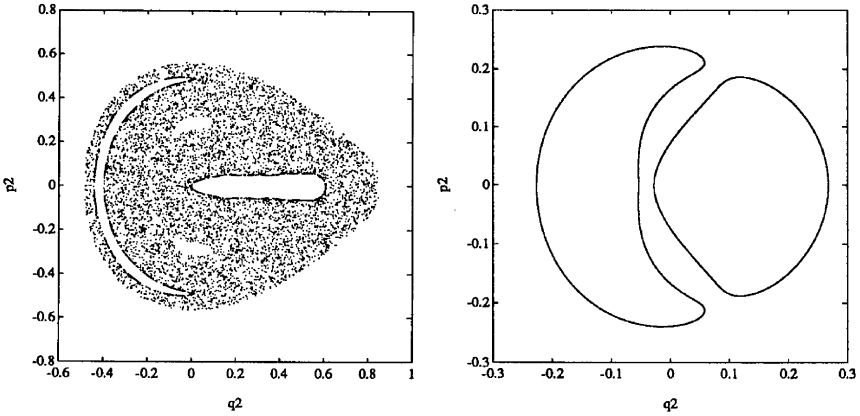

Fig. 1. Poincaré sections [15, pp. 12,13].

This system can be integrated using specially designed methods, for example the partitioned Runge–Kutta and certain Runge–Kutta–Nyström methods.

Hénon and Heiles (see [5]) formulated the Hamiltonian system

$$\frac{\mathrm{d}p_1}{\mathrm{d}t} = -(q_1 + 2q_1q_2), \quad \frac{\mathrm{d}p_2}{\mathrm{d}t} = -(q_2 + q_1^2 - q_2^2), \quad \frac{\mathrm{d}q_i}{\mathrm{d}t} = p_i, \quad i = 1,2 \tag{4}$$

with $d = 2$ but with only one conserved quantity, the Hamiltonian

$$T = \tfrac{1}{2}(p_1^2 + p_2^2), \qquad V = \tfrac{1}{2}(q_1^2 + q_2^2) + q_1^2q_2 - \tfrac{1}{3}q_2^3. \tag{5}$$

For later comparison, in Fig. 1, we show 'Poincaré cross sections' of Sanz-Serna and Calvo [5, pp. 12,13], intersections of the solution (p_2, q_2) with the plane $q_1 = 0$. The left figure corresponds to the initial condition IC1:

$$q_1 = q_2 = p_2 = 0, \quad p_1 = \sqrt{2H} \tag{6}$$

($H = 0.15925$) integrating to $t_{\mathrm{end}} = 3 \times 10^4$. In [5], this solution is described as 'randomly scattered' or 'chaotic' or 'stochastic'. The right figure depicts the corresponding 'quasiperiodic' Poincaré section for initial condition IC2:

$$q_1 = q_2 = p_1 = p_2 = 0.12 \tag{7}$$

($H = 0.029952$) generated by integrating to $t_{\mathrm{end}} = 2 \times 10^5$.

In the remainder of the paper, we introduce numerical methods for Hamiltonian problems and discuss the qualitative numerical phenomena observed in a variety of integrations of the Hénon and Heiles problem (4). In Section 2, we discuss a symplectic method used in a fixed-step integration and, in Section 3, a nonsymplectic method in a variable step integration. It is *not* intended that this discussion provides a comparison of the efficiency of the two types of methods. Such a comparison would require a more careful choice of methods.

Table 1
Fixed step RUTH4; initial condition IC1, DP

h	t_{end}	Poincaré	H error$_{max}$
0.200	3×10^4	C	5.27×10^{-4}
0.100	3×10^4	NC	2.31×10^{-5}
0.050	3×10^4	NC	1.42×10^{-6}
0.025	3×10^4	C	1.23×10^{-7}
0.010	3×10^4	C	3.16×10^{-9}
0.100	3×10^5	C	3.19×10^{-5}
0.050	3×10^5	C	1.98×10^{-6}

2. Symplectic methods

A discrete method is symplectic if it is a symplectic map. A symplectic map is one which, operating on any two-dimensional set D in the $2d$-dimensional space in which the system is formulated, preserves the sum of the areas of the projections of D onto the (p_i, q_i) planes. Symplectic discrete methods are often preferred as they have bounded Hamiltonian error.

For partitioned Hamiltonian systems, we can apply (explicit) partitioned RK (PRK) methods. We use a symplectic fourth-order PRK method (RUTH4) of [2,3], as implemented in the Fortran 90 code *new-hamint* [4].[1] (We have checked numerically that this implementation is fourth-order.) RUTH4 was used with initial condition IC1 and step sizes $h = 0.2, 0.1, 0.05, 0.025, 0.01$ in

(1) single precision (SP) with an approximate unit roundoff 1.19×10^{-7},
(2) double precision (DP) with an approximate unit roundoff 2.22×10^{-16},
(3) extended precision (EP) with an approximate unit roundoff 1.93×10^{-34}.

(Precision is adjusted simply using the "module" feature of Fortran 90.) Initial tests used double precision (see Table 1). For all step sizes except $h = 0.1$ and $h = 0.05$, the solution displays chaotic behavior (C) when integrating to $t_{end} = 3 \times 10^4$. Longer integrations (to $t_{end} = 3 \times 10^5$) using these step sizes also show chaotic behavior. The relative error in the Hamiltonian (Herror) is oscillatory; this relative error is computed over all output points. As anticipated, the maximum error decreases as h decreases. Fig. 2 depicts the Poincaré section for a typical chaotic solution ($h = 0.2$) while Fig. 3 shows the nonchaotic solution ($h = 0.1$). (The Poincaré section is computed by calculating the root of cubic Hermite interpolating polynomial fitted to the output values immediately on opposite sides of the section. Of course, the accuracy of the calculated section depends on the precision of the arithmetic and on the integration error.) Figs. 2 and 3 also present the corresponding relative Hamiltonian error showing the oscillatory behavior. Note, in Fig. 2, that the oscillatory band in the error widens around $t = 2.2 \times 10^4$, approximately where the chaotic behavior in the Poincaré section begins. For this reason the anticipated fourth-order behavior of the Hamiltonian error computed using the RUTH4 formula is not apparent in Table 1. In our computations, for all choices of h the quasiperiodic precedes the chaotic behavior. We computed a nonchaotic solution step size range

[1] The software used here, the integrator *new-hamint.f90* and a driver code for the Hénon–Heiles problem, may be accessed at the ftp site ftp.cygnus.math.smu.edu/pub/gladwell/new-hamint.f90.

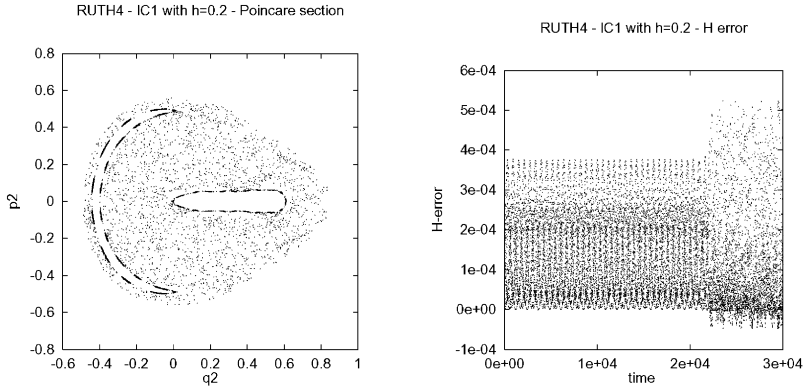

Fig. 2. RUTH4, $h = 0.2$, IC1, DP; Poincaré section and Hamiltonian error.

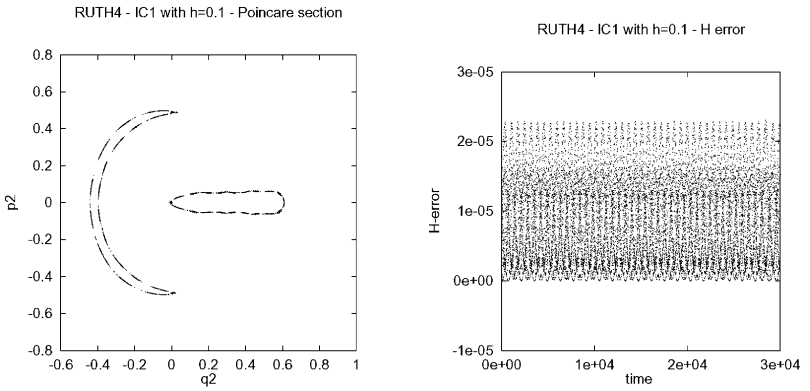

Fig. 3. RUTH4, $h = 0.1$, IC1, DP; Poincaré section and Hamiltonian error.

Table 2
Fixed step RUTH4; initial condition IC1, EP, $t_{\text{end}} = 3 \times 10^4$

h	Poincaré	H $\text{error}_{\max}$
0.10	NC	2.29×10^{-5}
0.05	C	1.98×10^{-6}
0.01	NC	2.27×10^{-9}

around $h = 0.1$, that is $0.099 < h < 0.102$. *That this range exists implies a real possibility of being deceived numerically about long-term solution behavior*.

Extended precision integration to $t_{\text{end}}=3\times10^4$ gives a nonchaotic solution around h=0.1 and h=0.01 but not at $h = 0.05$ (see Table 2), the Hamiltonian error is always oscillatory and essentially the same as for the double-precision calculation. Integrating further to $t_{\text{end}}=3\times10^5$ gives chaotic solutions for all three step sizes. In single precision, the relative Hamiltonian error is characterized by both low- and high-frequency oscillations (see Fig. 4). The corresponding Poincaré section is similar to that on the left of Fig. 2. A different step size, $h = 0.097$, produces an (isolated) nonchaotic solution.

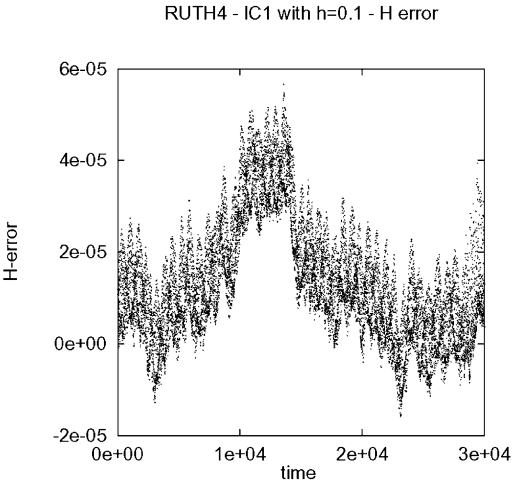

Fig. 4. RUTH4, $h = 0.1$, IC1, SP; Hamiltonian error.

Note that the effect of precision can be sufficient to induce different qualitative behaviors. For example, for $h = 0.1$ double and extended-precision integrations to $t_{\text{end}} = 3 \times 10^4$ are nonchaotic whereas single-precision integration is chaotic. Starting with the single precision initial values in both the double and extended-precision calculations still gives nonchaotic behavior. Looking more closely, if we compare the coordinates of corresponding points in the Poincaré sections then double- and extended-precision integrations agree to 15 digits initially but only to seven at the end. In contrast, double- and single-precision agree to seven digits initially but to no digits at the end of the integration, and the two integrations exhibit different qualitative behaviors.

In an extended-precision integration with $h = 0.05$, additional structures appear in the Poincaré section, particularly symmetrical (about the q_2 axis) clusters of points on the right side of the figure and an "envelope" for the section. Most of these features appear early in the integration; however, some do not, particularly the "envelope", but after a brief chaotic regime following the initial quasiperiodic regime. In Fig. 5, we show the results for an integration to $t_{\text{end}} = 3 \times 10^4$ and, in Fig. 6, for an integration to $t_{\text{end}} = 3 \times 10^5$. Note that, in general, the chaotic regime corresponds to the largest relative Hamiltonian errors and the smaller errors correspond to the initial quasiperiodic state and to later quasiperiodic states where structures internal to the section are computed. In contrast, the part of the integration where the envelope is computed is in the time period $t = (2.23\text{–}4.76) \times 10^4$ approximately, and *the relative Hamiltonian error is about the size seen in the chaotic regime*. Here again the sensitivity of the system may be observed. The qualitative features (the envelope and the special interior structures) may vanish if the initial value for p_1 is perturbed slightly. So, computing $p_1 = \sqrt{2H}$ in extended precision then solving the Hamiltonian system in extended precision leads to a rich set of structures. Just changing the initial value by computing it in double precision then solving the Hamiltonian system in extended precision is sufficient that the qualitative features are lost. The corresponding computations for initial condition IC2 are summarized in Table 3. The solution is quasiperiodic for both double and extended precision. Typically, for $h = 0.05$ (Fig. 7) the Poincaré section resembles that in [5]. For both double and extended precision, the relative error in the Hamiltonian oscillates, see Fig. 7 for $h = 0.05$.

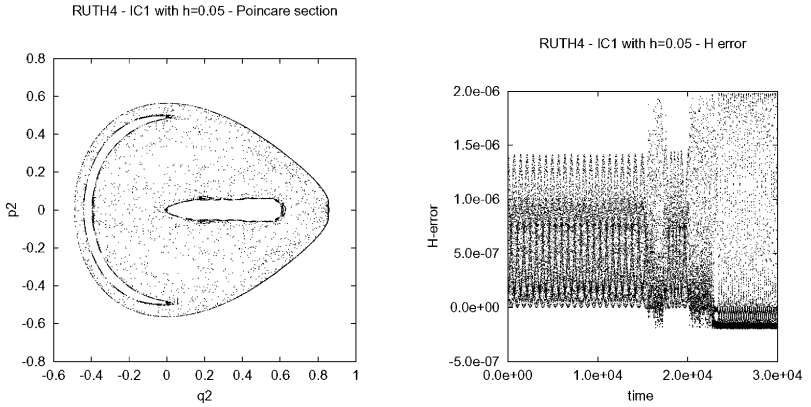

Fig. 5. RUTH4, $h = 0.05$, IC1, EP; Poincaré section, Hamiltonian error, $t_{\text{end}} = 3 \times 10^4$.

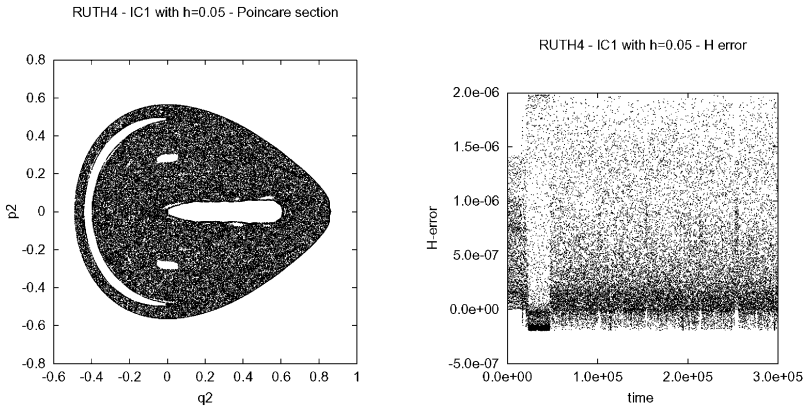

Fig. 6. RUTH4, $h = 0.05$, IC1, EP; Poincaré section, Hamiltonian error, $t_{\text{end}} = 3 \times 10^5$.

Table 3
Fixed step RUTH4; initial condition IC2, $t_{\text{end}} = 3 \times 10^5$

h	Precision	H $\text{error}_{\max}$
0.200	DP	1.61×10^{-4}
0.100	DP	9.74×10^{-6}
0.050	DP	6.04×10^{-7}
0.025	DP	3.77×10^{-8}
0.010	DP	9.64×10^{-10}
0.200	EP	1.61×10^{-4}
0.100	EP	9.74×10^{-6}

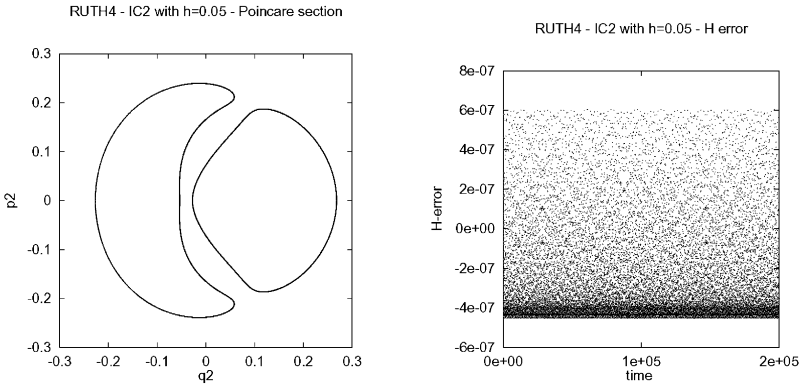

Fig. 7. RUTH4, $h = 0.05$, IC2, DP; Poincaré section and Hamiltonian error.

Table 4
Variable step RKL; initial condition IC1

Tolerance	t_{end}	Precision	Poincaré	H $error_{max}$
10^{-3}	3×10^4	DP	C	1.70×10^{-2}
10^{-4}	3×10^4	DP	C	1.66×10^{-3}
10^{-5}	3×10^4	DP	C	9.92×10^{-5}
10^{-5}	3×10^4	EP	NC	8.20×10^{-6}
10^{-6}	3×10^4	DP	C	4.97×10^{-6}
10^{-7}	3×10^4	DP	C	2.48×10^{-7}
10^{-8}	3×10^4	DP	C	1.12×10^{-8}
10^{-8}	3×10^4	EP	C	1.06×10^{-8}
10^{-9}	3×10^4	DP	C	5.49×10^{-10}
10^{-5}	3×10^5	EP	C	9.92×10^{-4}
10^{-8}	3×10^5	EP	C	1.18×10^{-7}
10^{-9}	3×10^5	EP	C	6.07×10^{-9}

3. Runge–Kutta–Nyström methods

We may integrate systems

$$\frac{\mathrm{d}\boldsymbol{p}}{\mathrm{d}t} = -\nabla_{\boldsymbol{q}} V = f(\boldsymbol{q}), \quad \frac{\mathrm{d}\boldsymbol{q}}{\mathrm{d}t} = \boldsymbol{p} \tag{8}$$

using nonsymplectic Runge–Kutta–Nyström methods as implemented in *new-hamint* [4]. Here we use RKL — a sixth-order explicit method with a fourth-order embedded error estimate, originally developed for integrating the special second-order systems of celestial mechanics [1].

Results for initial condition IC1 are given in Table 4. All Poincaré sections are chaotic except for the isolated instance of the extended-precision integration at tolerance $= 10^{-5}$, for which the section (see Fig. 8) is concentrated around the quasiperiodic structure in Fig. 3 but with more 'spreading' than in Fig. 1. A refined search (near tolerance $= 10^{-5}$) for other nonchaotic solutions failed to reveal any.

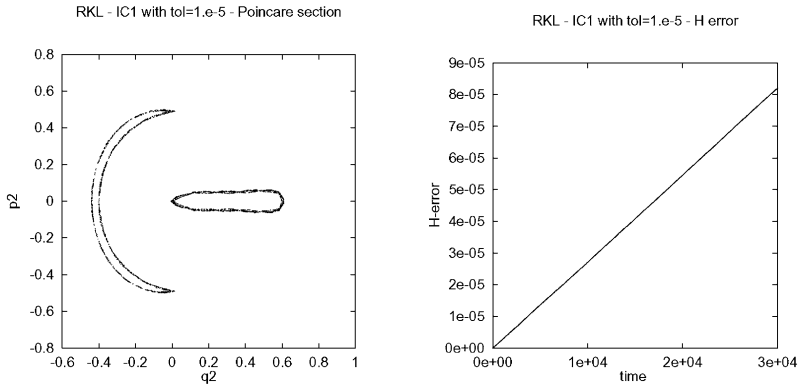

Fig. 8. RKL, tolerance $= 10^{-5}$, IC1, DP; Poincaré section and Hamiltonian error.

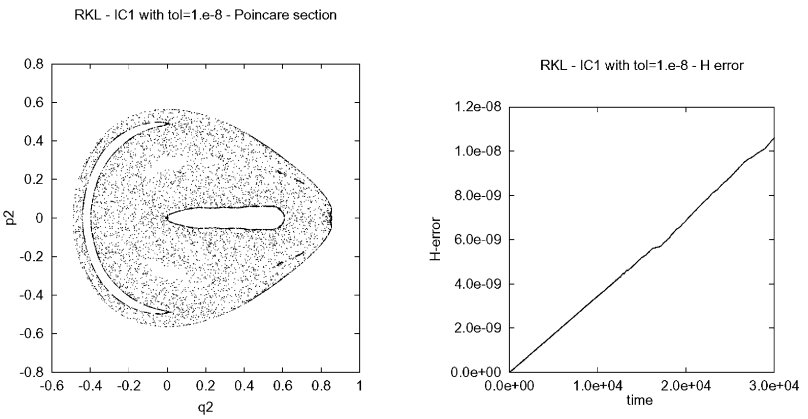

Fig. 9. RKL, tolerance $= 10^{-8}$, IC1, EP; Poincaré section and Hamiltonian error.

In Fig. 8 the Hamiltonian error has an almost linearly increasing trend on which a small oscillation is superposed. This behavior is observed in all accurate integrations in double and extended precision throughout the quasiperiodic regime. For less-accurate integrations this behaviour is less marked and does not appear immediately. Particularly, the oscillations are flatter for the less accurate integrations. Fig. 9 shows a chaotic case in extended precision for tolerance$=10^{-8}$. Linear changes with superposed oscillations in the relative Hamiltonian error in the quasiperiodic regimes are observable, as in other similar integrations. See the left figure in Fig. 10 which presents a detail of the error for a typical double precision case for the range $t = 0$–10^3. This is a macroscopic view of the error. At the microscopic level, within a single oscillation there are (mainly) small differences in error behavior. These are most marked at relaxed tolerances. In the chaotic regime the relative Hamiltonian error is essentially linearly increasing (without superposed oscillations); the average slope of the error is slightly greater in the chaotic regime than in the quasiperiodic regime. In addition, other features (slope changes and flat regions) are observed; see the right figure in Fig. 10 which presents a detail of the error for a typical extended-precision case for the range $t = (1.2$–$1.8) \times 10^4$. These correspond

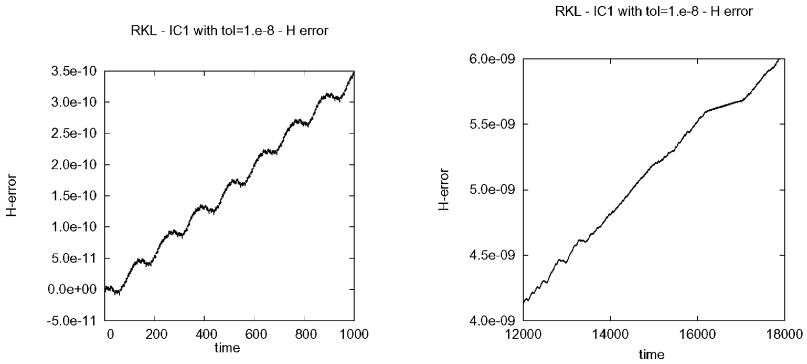

Fig. 10. RKL, tolerance $= 10^{-8}$, IC1; Hamiltonian error detail.

Table 5
Variable step RKL; initial condition IC2, $t_{end} = 3 \times 10^5$, DP

Tolerance	H $error_{max}$
10^{-3}	5.51×10^{-2}
10^{-4}	6.04×10^{-3}
10^{-5}	4.25×10^{-4}
10^{-6}	2.59×10^{-5}
10^{-7}	1.21×10^{-6}
10^{-8}	5.49×10^{-8}
10^{-9}	3.02×10^{-9}

to the appearance of additional structures in the Poincaré section, particularly symmetrical (about the q_2 axis) clusters of points on the right side of the figure and an "envelope" for the section partially completed on the right. These features appear early in the integration. However, some features do not appear at the beginning of the integration, particularly the "envelope", but after a brief chaotic regime following the initial quasiperiodic regime.

Table 5 displays the results for initial condition IC2. All tolerances produce a quasiperiodic solution similar to that on the right of Fig. 1 and to that obtained with the fixed step size RUTH4 (Fig. 7). The relative Hamiltonian error has a similar linear with superposed oscillations behavior as that seen in Fig. 10. *We observe that for given initial conditions, the number of oscillations in the error per unit time seems approximately constant*. Of course, the size of the error at a given time depends almost linearly on the tolerance. So, for initial conditions IC1 and any tolerance we observe almost eight oscillations per thousand units of time. For IC2, the corresponding number is close to two.

In either Table 4 or Table 5, plotting the logarithm of the maximum error against the logarithm of required tolerance, a closely fitted straight line has slope slightly greater than one, i.e., close to *tolerance proportionality*. Assuming that when we measure the error we are already in the final integration regime, this enables us to predict a tolerance to control the Hamiltonian error below a given threshold for a given time interval.

References

[1] R.W. Brankin, J.R. Dormand, I. Gladwell, P.J. Prince, W.L. Seward, Algorithm 670: a Runge–Kutta–Nyström code, ACM Trans. Math. Software 15 (1989) 31–40.
[2] J. Candy, W. Rozmus, A symplectic integration algorithm for separable Hamiltonian functions, J. Comput. Phys. 92 (1991) 230–256.
[3] E. Forest, R.D. Ruth, Fourth-order symplectic integration, Physica D 43 (1990) 105–117.
[4] I. Gladwell, K. Bouas-Dockery, R.W. Brankin, A Fortran 90 separable Hamiltonian system solver, Appl. Numer. Math. 25 (1997) 207–217.
[5] J.M. Sanz-Serna, M.P. Calvo, Numerical Hamiltonian Problems, Chapman & Hall, London, 1994.